Polymorphism in phase-change materials: melt-quenched and as-deposited amorphous structures in $Ge_2Sb_2Te_5$ from density functional calculations

J. Akola,[1,2,3] J. Larrucea,[3] and R. O. Jones[1,4]

[1]*Institut für Festkörperforschung, Forschungszentrum Jülich, D-52425 Jülich, Germany*
[2]*Department of Physics, Tampere University of Technology, P.O. Box 692, FI-33101 Tampere, Finland*
[3]*Nanoscience Center, Department of Physics, P.O. Box 35, FI-40014 University of Jyväskylä, Finland*
[4]*German Research School for Simulation Studies, FZ Jülich and RWTH Aachen, D-52425 Jülich, Germany*

(Received 15 December 2010; revised manuscript received 11 January 2011; published 10 March 2011)

The as-deposited (AD) amorphous structure of the prototype phase change material $Ge_2Sb_2Te_5$ (GST-225) has been studied by density functional calculations for a 648-atom sample generated by computer-aided deposition at 300 K. The AD sample differs from a melt-quenched (MQ) sample in essential ways: (1) Ge atoms are predominantly tetrahedrally coordinated, and (2) homopolar and Ge-Sb bonds are more common and reduce the number of $ABAB$ squares (A = Ge, Sb; B = Te), the characteristic building blocks of the material. The first observation resolves the contradiction between measured (EXAFS) and calculated Ge-Te bond lengths, and the latter explains the very different crystallization speeds. Sb and Te have higher chemical coordination than suggested by the "8-N rule" of covalent networks (N is the number of valence electrons). The EXAFS signal calculated for AD agrees much better with experiment than that calculated for MQ.

DOI: 10.1103/PhysRevB.83.094113 PACS number(s): 61.43.Dq, 61.46.−w, 61.43.Bn, 71.15.Pd

I. INTRODUCTION

Amorphous films play central roles in many areas of science and technology, and it is common to find dramatically different properties in as-deposited (AD, vapor deposition, sputtering) and melt-quenched (MQ, annealed) samples of the same material. Examples include stable glasses of indomethacin, where vapor deposition is viewed as a route to find "hidden" amorphous states,[1] thermally induced changes in the refractive index of As-S glasses,[2] and amorphous magnetic films such as $Fe_{80}B_{20}$.[3] These differences are profound and important in phase change materials (PCM), which are used in rewritable data storage, such as Digital Versatile Disk–Random Access Memory (DVD-RAM) and Blu-ray Disc (BD).[4] PCM are chalcogenide alloys that utilize the rapid and reversible transition between amorphous and crystalline phases of nanosized marks in thin polycrystalline films. The transition can occur in nanoseconds by heating above the glass transition temperature, and the states can be identified by their optical properties and resistivity. The rate-limiting step in the read/erase cycle is (re)crystallization of the nanosized bits. MQ samples of many PCM crystallize much faster than AD samples,[5–8] so it is a challenge to determine both amorphous structures and discover why they behave differently. We address these problems here.

The most common PCM are GeTe-Sb_2Te_3 pseudobinary compounds, particularly $Ge_2Sb_2Te_5$ (GST), and doped Sb_xTe alloys ($x > 2$). Extended x-ray absorption fine structure (EXAFS) data,[9–11] x-ray diffraction (XRD) measurements,[12] and x-ray photoelectron spectra (XPS)[13] have provided important clues to the atomic structure of a-GST, but the local coordination of Ge atoms remains controversial: EXAFS indicates shorter Ge-Te bonds (2.61–2.63 Å) than in the crystal, which may indicate sp^3 hybridization and tetrahedral coordination, while XRD favors octahedral bond angles for all atom types, which leads to longer Ge-Te bonds.[12] Density functional (DF) calculations[14–19] generally support the latter view (calculated bond lengths are 2.77–2.78 Å, with some tetrahedral Ge atoms) and have identified $ABAB$ rings (A = Ge, Sb; B = Te) as the main structural units. It is difficult to prepare MQ samples of the required size, so their structures have been compared experimentally only very recently.[20] A crucial question remains: Are theory and experiment studying the same structural phase (polymorph)?

We report DF/molecular dynamics (MD) simulations of a 648-atom sample of a-GST generated by computer-aided deposition on a 2D template and compare with our earlier results for an MQ sample (460 atoms), refined with respect to XRD and XPS data with reverse Monte Carlo (RMC).[18] AD and MQ have similar structures and electronic properties, but the former has many tetrahedral Ge atoms and numerous "wrong bonds" (homopolar and Ge-Sb bonds) that hamper crystallization. Our AD results agree with EXAFS measurements[9,10] and explain the apparent inconsistency of earlier calculations of Ge-Te bond lengths. Our technique should be applicable to generating the AD amorphous structures of other PCMs and semiconductor alloys.

II. DETAILS OF CALCULATIONS

The calculations with the CPMD program (Born-Oppenheimer mode)[21] use scalar-relativistic Troullier-Martins pseudopotentials,[22] periodic boundary conditions with a single point ($\mathbf{k} = 0$) in the Brillouin zone, and a kinetic energy cutoff of the plane wave basis of 20 Ry (additional calculations for the pressure tensor are performed with 40 Ry). The PBEsol functional[23] is used for the exchange-correlation energy, since it often gives better results for extended systems than other generalized gradient approximations. We use a Nosé-Hoover thermostat (frequency 800 cm^{-1}, chain length 4)[24] for molecular dynamics and a stable and efficient predictor-corrector algorithm for wave function optimization.[25] Simulations are

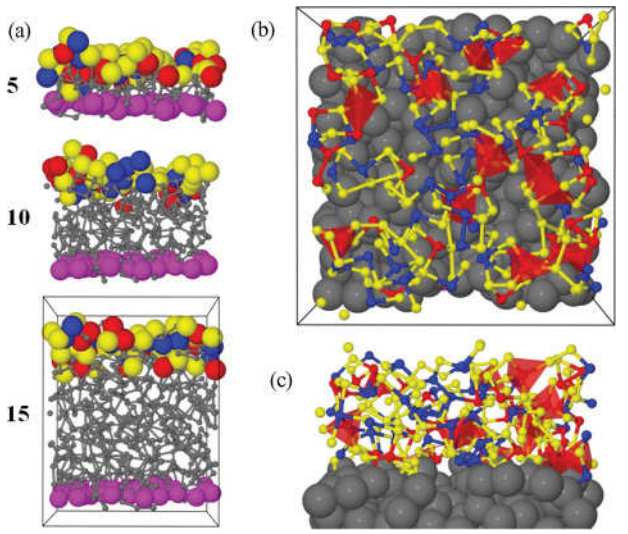

FIG. 1. (Color online) Deposition at 300 K. (a) After 5, 10, and 15 added layers. Two topmost layers (72 atoms, relaxed) are shown in color. Magenta spheres (lowest layer): The 32 atoms that are fixed upon deposition. Ge, red (gray); Sb, blue (black); and Te, yellow (white). (b) Top view after 17 added layers (648 atoms). The atoms within 1.2 nm are highlighted, and red (gray) tetrahedra show tetrahedrally coordinated Ge atoms. (c) Side view of final sample.

performed for a fixed volume (NVT ensemble) for each step of sample generation and data collection.

The simulations were performed at 300 K, beginning with a random template of 36 atoms (8 Ge, 8 Sb, and 20 Te) in an area of 27.61 × 27.61 Å^2 (layer thickness 1.4 Å). These atoms were fixed during deposition in order to avoid significant relaxation in the lower part of the system. 17 sparse layers of 36 atoms (random coordinates, initial thickness 4 Å) were then deposited and allowed to relax for 5–10 ps. The vertical box dimension was adjusted for each layer to minimize the interaction with its replica (vacuum region 10 Å). The process is summarized in Fig. 1. Despite the relatively low temperature, mixing between layers occurs, and the lower coordination of Te enhances its concentration at the surface. The final vertical dimension of the 648-atom sample is 15% greater than in the bulk. The model AD system was then prepared by releasing the 32 template atoms and decreasing the vertical box size (19 steps at 300 K) to obtain a cubic supercell (size 27.61 Å, density 0.0308 atoms Å^{-3}). The process lasted 67 ps in steps of 3–4 ps, and the system was equilibrated for 34 ps before final data collection (25 ps). The pressure was small (2.9 ± 1.8 kbar) at the final (experimental) density, and the structure was then optimized at 0 K.

The structure of the MQ sample (460 atoms) was based on the recent RMC-refined geometry,[18] which reproduced the XRD structure factor $S(Q)$ of the AD sample and has a semiconducting band gap. This does not have the lowest DF energy, so we performed a simulation at 300 K with the same functional (PBEsol) and atomic density as in AD. Initialization (5 ps, 300 K) was followed by data collection (35 ps), and properties of AD and MQ are given in Table I. MQ is 11 meV/atom *more stable* than AD and 58 meV/atom less stable than the rocksalt structure.

TABLE I. Properties of AD and MQ. r_0 ($r_{\min}$): first maximum (minimum) in PDF, N: total coordination number (bond cutoff 3.2 Å, values in parentheses are the chemical coordination), f_{ABAB}: fraction of atoms in $ABAB$ squares, V_c: fraction of cavities, P: pressure, ΔE_{coh}: cohesive energy difference, E_g: band gap.

Sample	AD	MQ	Expt. (AD)[a]
No. atoms	648	460	
$r_{\text{Ge–Ge}}$ (Å)	2.52	2.55	2.47 ± 0.03
$r_{\text{Ge–Te}}$ (Å)	2.69	2.72	2.63 ± 0.01, 2.61 ± 0.01[b]
$r_{\text{Sb–Te}}$ (Å)	2.89	2.89	2.83 ± 0.01, 2.85 ± 0.01[b]
N(Ge)	4.15 (3.80)	4.14 (3.70)	3.9 ± 0.8
N(Sb)	3.72 (3.63)	3.71 (3.62)	2.8 ± 0.5, 3.3 ± 0.6
N(Te)	2.76 (3.12)	2.83 (3.13)	2.4 ± 0.6
f_{ABAB} (%)	35.2	52.5	
V_c (%)	16.3	14.3	
P (kbar)	2.9 ± 1.8	1.0 ± 2.3	
ΔE_{coh} (meV)	0.0	11.7	
E_g (eV)	0.18	0.26	

[a]From Ref. 10 if not otherwise stated.
[b]From Ref. 9.

III. RESULTS

Figure 2 shows the final (gradually compressed) structure of the AD sample from two perspectives. The cubic unit cell has a side of 27.61 Å. Cavities (shown by cyan isosurfaces) are defined by analogy to Voronoi polyhedra in amorphous solids[14] and comprise 16.3% of the total volume. The cavities are located using a test particle of radius 2.8 Å.

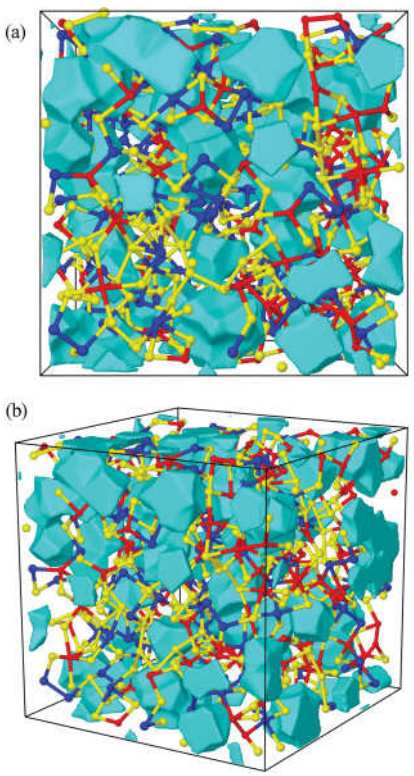

FIG. 2. (Color online) Final AD sample of GST at 300 K from two perspectives. Red (gray): Ge, blue (black): Sb, yellow (white): Te. Cavities are also shown.

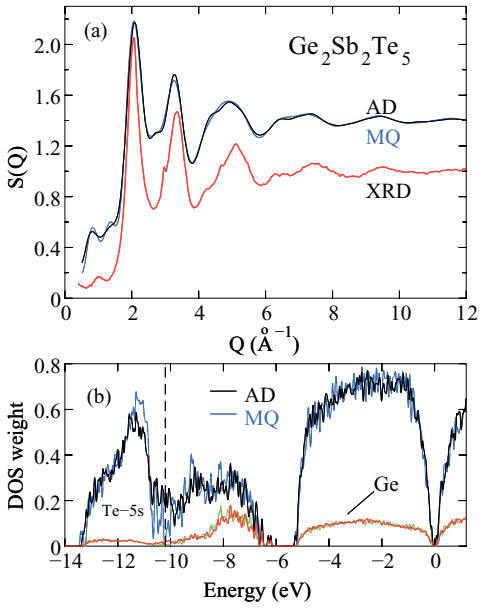

FIG. 3. (Color online) (a) The structure factors of AD (black) and MQ (blue) at 300 K are almost indistinguishable. XRD data shown in red (gray). Calculated curves were shifted by 0.4. (b) Electronic DOS of AD and MQ and the projection (p-DOS) onto Ge atoms (AD, red; MQ, green) are also very similar. The vertical dashed line denotes the gap between the σ bands.

A. Structure factors, pair distribution functions, electronic DOS

The structure factors $S(Q)$ of AD and MQ [Fig. 3(a)] are strikingly similar, and transition electron microscopy experiments[20] confirm that it is difficult to distinguish between them using diffraction techniques alone. The agreement with experiment is very good, although the calculated peaks at 2.1 and 3.3 Å^{-1} are a little low, and the shape of the third peak differs slightly. The calculations reproduce the prepeak at 0.9–1.0 Å^{-1}, and the PBEsol functional leads to shorter bonds.[18] The electronic densities of states (DOS) for AD and MQ are very similar [Fig. 3(b)], with band gaps of 0.2–0.3 eV at the Fermi energy, in reasonable agreement with XPS data.[13] The DOS minimum at −10.2 eV between two σ-bands is weaker in AD, since the neighboring peak (with Te-5s character) is less pronounced when Te-Te bonds are formed (see the first Te-Te peak in Fig. 4). This is consistent with the measured XPS profile, and the computed inverse participation ratios (Sec. III F) show that the corresponding states are more localized. The projections onto atomic orbitals (p-DOS), shown for Ge, are not significantly different for AD and MQ.

The partial distribution functions (PDFs) are shown in Fig. 4. Ge-Te and Sb-Te bonds dominate in GST ("AB alternation"), and the insets show the first peaks in detail. We have noted above the apparent contradiction between EXAFS measurements (short Ge-Te bonds suggesting tetrahedral coordination)[9–11] and XRD measurements and DF simulations (longer Ge-Te bonds and distorted octahedral coordination).[14–16] The discrepancy appears to have two causes: (a) E_{xc} functionals tend to overestimate bond distances by 2%– 3%, and the PBEsol approximation gives better results (the Ge-Te PDF maximum in MQ is at 2.72 Å). (b) Sample

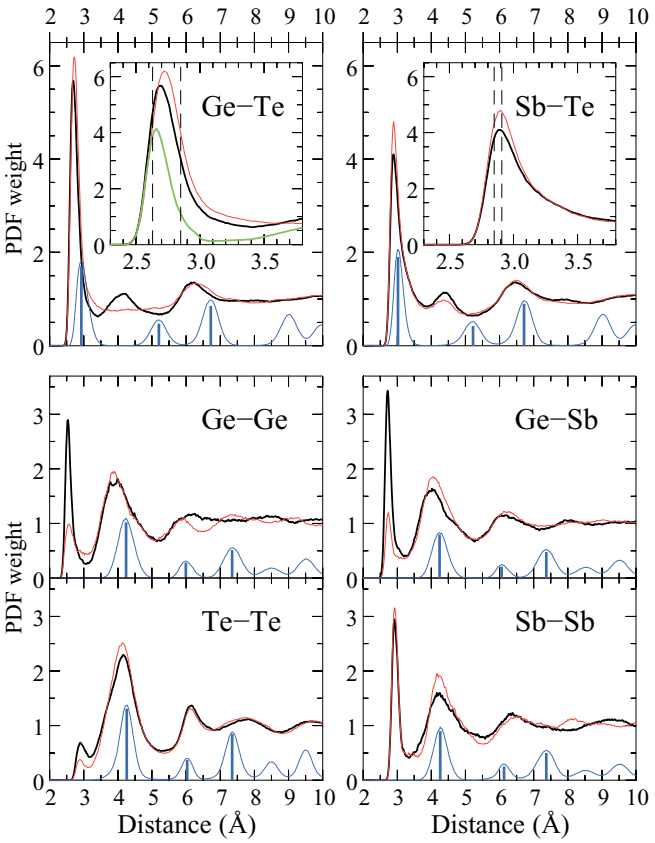

FIG. 4. (Color online) PDFs of AD (thick black) and MQ [red (gray)] a-GST at 300 K. Lowest curves [blue (thin black)]: c-GST at 300 K (scaled by 0.25). Insets: Ge-Te and Sb-Te bonds. Dashed lines: EXAFS measurements for a- and c-GST. Green (light gray): Tetrahedral Ge-Te bonds.

preparation is crucial: AD has more tetrahedral Ge atoms than MQ, and the Ge-Te maximum shifts to 2.69 Å. Finally, tetrahedral structures have a PDF maximum at 2.65 Å, only 1% greater than experiment. This is consistent with PBEsol calculations of semiconductor lattice constants.[23] Ge-Ge bond lengths (2.52 Å), corresponding here mainly to tetrahedral Ge atoms, agree well with experiment.

Sb-Te bond lengths change little on amorphization, and both AD and MQ have the first maximum at 2.89 Å. The other PDFs are distinctly different, as the number of "wrong bonds," i.e., homopolar and Ge-Sb bonds that do not occur in c-GST, is much larger in AD. This is reflected also in the Ge-Te and Sb-Te PDFs (AB bonds) as weaker first maxima and emerging second maxima (humps) at 4.2 Å.

B. Bond angle distributions

The bond angle distributions around each element (Fig. 5) reveal details of the local environment. The X-Sb-X bond angle distribution [Fig. 5(b), X any atom] shows characteristic octahedral bond angles with a narrow peak at 90° and enhanced weight for nearly linear configurations (180°). AD and MQ differ little in this respect. For Te, the maximum around 90° again dominates, but the weight is small above 120°. The X-Te-X distributions differ in the two samples. The X-Ge-X distributions resemble those of Sb, but their maxima are

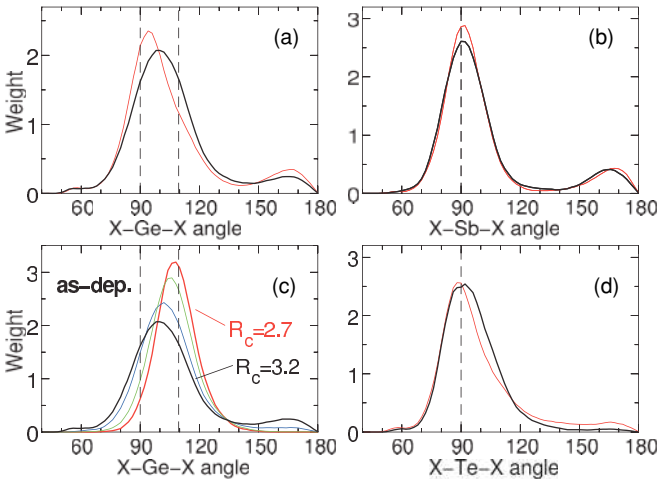

FIG. 5. (Color online) Bond angle distributions of AD (black) and MQ [red (gray)] for bond cutoff of 3.2 Å. Vertical dashed lines denote octahedral (90°) and tetrahedral (109.47°) values. (c) The effect of changing cutoff from 2.7 to 3.2 Å for Ge-centered configurations.

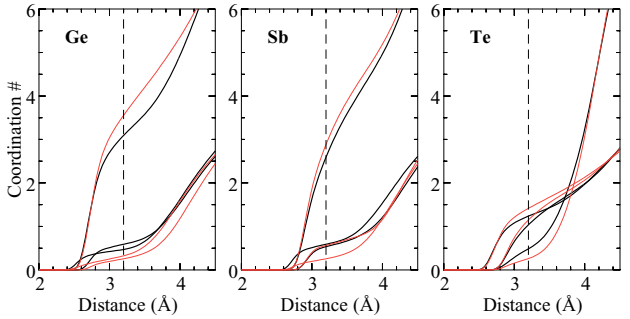

FIG. 6. (Color online) Integrated partial coordination numbers around Ge, Sb, and Te. Thick black: AD, thin red (gray): MQ. The partial PDFs with Ge have the shortest threshold in each panel. Vertical dashed line: bond cutoff distance (3.2 Å).

shifted to larger values (MQ: 94°, AD: 100°) and are broader [Fig. 5(a)].

The shift of the X-Ge-X distributions toward the tetrahedral value (109.47°) is shown in Fig. 5(c), where the bond cutoff is varied from 2.7 to 3.2 Å. The restriction to bonds shorter than 2.7 Å leads in AD to a maximum consistent with tetrahedral configurations.

C. Coordination numbers and bond orders

The partial coordination numbers (Table II) have been determined using a cutoff radius of 3.2 Å, as were the values in Table I. Figure 6 shows the partial coordination numbers as a function of cutoff radius for each bond type. The AD and MQ samples differ, particularly in the homopolar and Ge-Sb connections, where the former has more weight near the threshold. Te-Te bonds are rare but contribute more in the region of second-nearest neighbors (above 4 Å). Table II shows that Ge and Sb have twice as many wrong bonds (1.1 on average) as Te (with Te-Te bonds), although more than half of the atoms are Te. Random deposition does not favor particular bond configurations, and this is further evidence of the unfavorable nature of Te-Te bonds in *a*-GST.

The differences between Ge-centered bond angles [Fig. 5(a)] raises the question: Do the numbers of tetrahedrally coordinated Ge atoms differ in the two samples? We find that *fourfold* coordination is larger in AD (70%) than in MQ (59%). The fraction of tetrahedrally coordinated[26] Ge atoms at 300 K is significantly higher in AD (58%) than in MQ (36%). The fraction of tetrahedral atoms in the optimized structures at 0 K (AD: 71%, MQ: 42%) shows that thermal fluctuations lower this fraction (fourfold coordination has a higher weight, in general).

TABLE II. Partial coordination numbers. Values in parentheses correspond to $n_{\mathrm{Te-Ge}}$ and $n_{\mathrm{Te-Sb}}$, respectively.

Sample	AD	MQ	Expt. (AD)[a]
$n_{\mathrm{Ge-Ge}}$	0.47	0.33	0.6 ± 0.2
$n_{\mathrm{Ge-Sb}}$	0.59	0.26	
$n_{\mathrm{Ge-Te}}$	3.09 (1.23)	3.55 (1.42)	3.3 ± 0.5
$n_{\mathrm{Sb-Sb}}$	0.54	0.56	
$n_{\mathrm{Sb-Te}}$	2.59 (1.04)	2.88 (1.15)	2.8 ± 0.5
$n_{\mathrm{Te-Te}}$	0.49	0.26	

[a]From Ref. 10.

Chemical bond orders (strengths) have been calculated for all atoms by wave function projections (99.9 % complete) onto atomic *s*-, *p*-, and *d*-orbitals. The chemical coordination numbers (Table I) were obtained by summing the bond orders for individual atoms. The distributions for Ge-Te and Sb-Te bonds for *a*- and *c*-GST (Fig. 7) show that the maxima of the amorphous phase are shifted toward 1, the value for a single covalent bond. The crystalline material has broad maxima between 0.4 and 0.8, and a weaker covalent character. The increased weight near 0 is due to nonbonded atoms (e.g., second-nearest neighbors).

Earlier calculations of PDFs[14,15,18] in *a*-GST showed that the total coordination numbers of Sb and Te do not follow the "8-*N* rule" of covalently bonded networks (Table I), and this is supported by calculations of bond orders (number of chemical bonds) from the overlap of wave functions for each bond. The Ge-Te and Sb-Te bond orders have maxima at 0.9, indicating nearly covalent single bonds (unity)[19] that are shifted from the broader *c*-GST maxima (∼0.6). This reflects the changes in the electronic properties upon crystallization and is coupled to the medium range order (Jahn-Teller deformation in *c*-GST, resonance effects).[27] The chemical coordination of Ge, Sb, and Te is 3.7–3.8, 3.6, and 3.1 for AD and MQ; Sb and Te are clearly overcoordinated.

D. Local order parameters

The discussion of nearest neighbor topology is aided by separating the atoms into types *A* (Ge, Sb) and *B* (Te). In *c*-GST, all *A* atoms are coordinated octahedrally to *B*, and this feature has been used to define an order parameter α.[14] The contribution of atom i of type A is written

$$\alpha_i^{(A)} = \frac{1}{n_B} \sum_{j \neq i} f(r_{ij}) \frac{\sum_{k \neq i,j} |f(r_{ik})| g(\theta_{ijk})}{\sum_{k \neq i,j} |f(r_{ik})|}, \qquad (1)$$

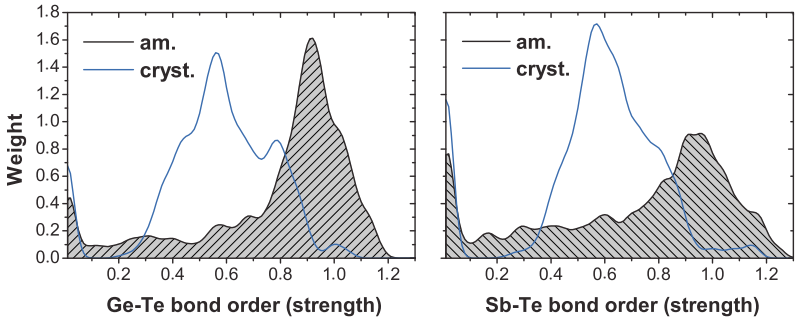

FIG. 7. (Color online) Bond order distribution of Ge-Te and Sb-Te bonds in amorphous (shaded) and crystalline (blue line) GST.

where n_B is the number of nearest neighbors of type B in the rocksalt structure (6). A similar formula holds for contributions from type B (Te) atoms. $f(r_{ij})$ is the cutoff distance for counting nearest neighbors, and its sign depends on bond type,

$$f(r_{ij}) = \frac{\pm 1}{\exp[\kappa^{-1}(r_{ij} - r_0)] - 1}, \tag{2}$$

and $g(\theta_{ijk})$ is the angular weighting function:

$$g(\theta_{ijk}) = \cos^2[2(\theta_{ijk} - \theta_0)]. \tag{3}$$

A-A and B-B bonds ("wrong bonds") give negative contributions, and type A atoms with octahedral coordination to A atoms contribute -1. The order parameter is unity for the rocksalt structure with AB alternation and vanishes for a completely disordered system. The parameters ($r_0 = 3.2$ Å, $\kappa = 0.05$ Å, $\theta_0 = 90^\circ$) provide a smooth bond cutoff and reduce the order parameter when the bond angle θ_{ijk} deviates from the angles favored in the rocksalt structure (90° and 180°).

Figure 8 shows the local order parameters α_i for Ge and Sb in the AD and MQ samples. While the Ge color maps differ for the two samples, the Sb plots are remarkably similar. For Sb, the increased number of homopolar bonds is reflected in the region around [4, 0] which corresponds to fourfold coordination with two "wrong bonds" (AB-2) for each atom. The fraction of atoms f_{ABAB} that occur in $ABAB$ rings (Table I) shows that there are fewer in AD.

The Ge order parameters have maxima [(4,0.4), (4,0.2), and (4,0.1)] corresponding to tetrahedral bond angles, depending on the bond types. The tetrahedral order parameter q_i,[15]

$$q_i = 1 - \frac{3}{8}\sum_{j>k}\left[\cos\theta_{ijk} + \frac{1}{3}\right]^2, \tag{4}$$

is shown for Ge in Fig. 9 for different coordination numbers. For fourfold coordination, it has the values 1 and 0.625 for tetrahedral and (distorted) octahedral configurations, respectively, and emphasizes tetrahedral coordination, not the type of the neighbors.[15] There are more tetrahedral Ge atoms in AD (58%) than in MQ (36%).[26] Deposition begins with low-coordinated surface atoms (at smaller density) and favors fourfold coordination (70%). Ge atoms are then likely to adopt

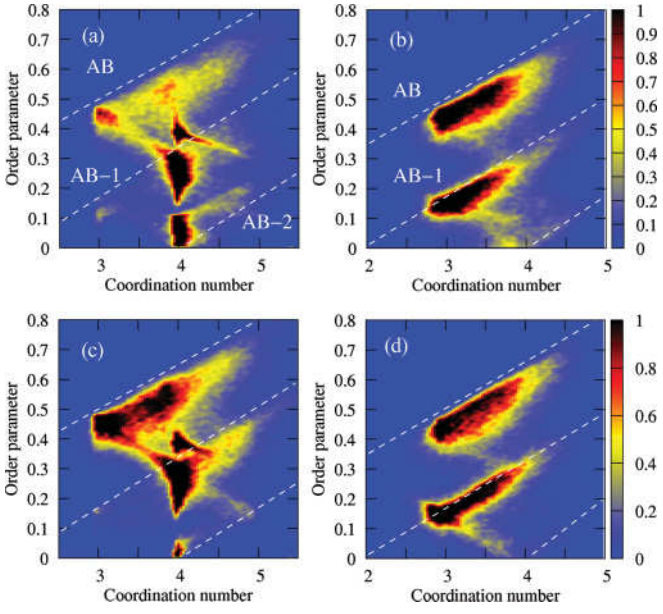

FIG. 8. (Color online) (a)–(b) Color maps of order parameter α_i for (a) Ge and (b) Sb in AD at 300 K. (c)–(d) The same for MQ. The color scales of the two samples have been calibrated for Ge and Sb separately to maximize clarity.

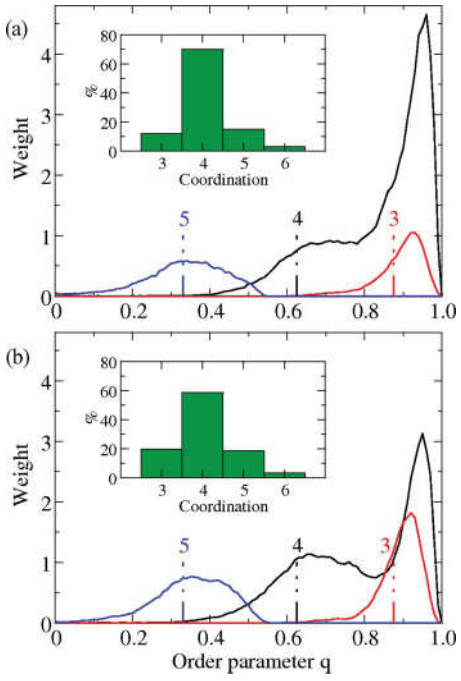

FIG. 9. (Color online) Tetrahedral order parameters q_i for total coordination 3, 4, and 5. (a) AD. (b) MQ. Vertical dot-dashed lines denote octahedral bond angles, and insets show distributions of coordination numbers.

a tetrahedral coordination, as shown in Fig. 1(c) near the sample surface.

E. EXAFS signal

The EXAFS signal $\langle\chi_\alpha(k)\rangle$ observed at the edge of atom type α is the sum of contributions from all types β integrated over the corresponding partial pair distribution functions $g_{\alpha\beta}(r)$:

$$\langle\chi_\alpha(k)\rangle = \sum_\beta \int_0^\infty dr\ 4\pi r^2 \rho_\beta\ g_{\alpha\beta}(r)\ \gamma^{(2)}_{\alpha\beta}(k,r), \qquad (5)$$

where ρ_β is the average atomic density of type β. The pair signal $\gamma^{(2)}_{\alpha\beta}(k,r)$ is usually approximated by the single scattering contribution,[28] which involves the phase shifts of the scattering ions. These were calculated for Ge, Sb, and Te atoms using the muffin-tin approximation (radii Ge: 2.3 Å, Sb: 2.6 Å, Te: 2.7 Å) and the Hedin-Lundqvist complex potential for the excited state. The overlap of the valence charge densities was simulated by a representative bonding environment, and the core-hole lifetimes were included in the imaginary part of the potential. The EXAFS signals were computed with the program GNAMX[28,29] from the calculated partial pair distribution functions. The PDF were multiplied beyond 3.5 Å by a half Gaussian cutoff function ($\sigma = 0.7$ Å) in order to smooth higher frequency contributions. The k scale was obtained by shifting the theoretical energy scale by $\Delta E = +0.8$ Ry to align the vacuum levels.

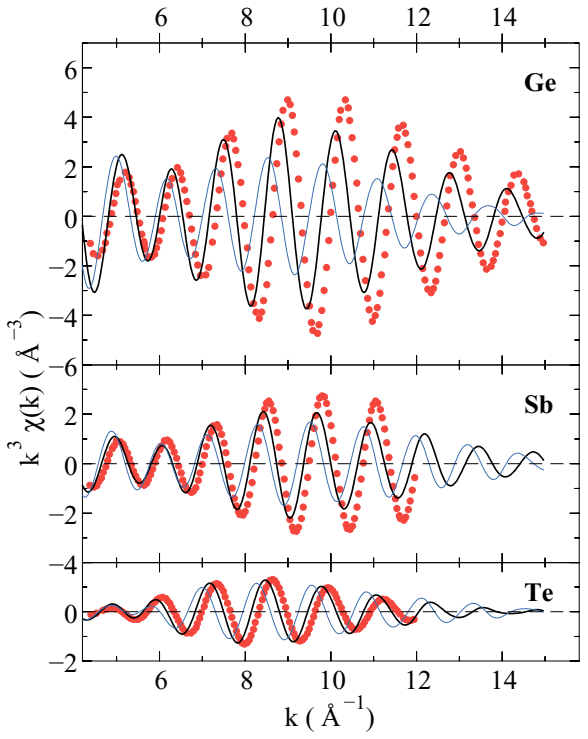

FIG. 10. (Color online) EXAFS signal of the Ge, Sb, and Te K-edge. Black curve: AD sample (this work), thin blue (black) curve: MQ simulation (460 atoms), dots [red (gray)]: experimental results [Ref. 11].

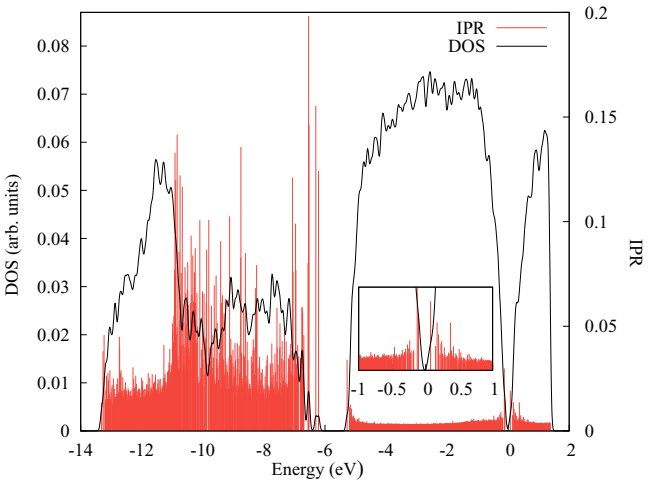

FIG. 11. (Color online) Electronic density of states (DOS) of the AD. The inset shows close-up of the regions near the Fermi energy (0 eV). The inverse participation ratios for each KS orbital are shown by red (gray) lines.

A comparison of the calculated EXAFS spectra with experimental data[11] (Fig. 10) shows that our AD model with 648 atoms is a definite improvement over the initial MQ model (460 atoms).[14] The phase of oscillations and amplitude for Ge correspond much better, and the Sb and Te signals are also improved. The Ge signal is consistent with the increased number of tetrahedral Ge atoms and better E_{xc} functional, which together result in shorter Ge-Te (and Ge-Ge) bonds. The Sb-Sb and Sb-Te (Te-Te) bonds are reduced slightly. We emphasize that the calculation is a DF result without additional fitting to experiment.

F. Inverse participation ratio

The degree of localization of the single-particle Kohn-Sham functions $\psi(\mathbf{r})$ can be determined by the inverse participation ratios (IPR):

$$\mathrm{IPR} = \frac{\int d\mathbf{r}|\psi(\mathbf{r})|^4}{\left(\int d\mathbf{r}|\psi(\mathbf{r})|^2\right)^2}. \qquad (6)$$

Delocalized orbitals have small values, and a large value indicates localization around specific (covalent) bond(s). The IPRs (Fig. 11) were calculated from the projections of the KS functions onto an atomic basis set (see Sec. III C), using the related atomic orbital coefficients in the integral (summation).

Figure 11 emphasizes the localized nature of the KS states in the region of Te-5s character (around -10 to -11 eV), and in the upper edge of the σ band above -7 eV (where the Ge-5s character dominates). The large localization in the former is related to Te-Te bond formation and to the increased overlap of the atomic orbitals of Te and Sb. The AD sample has more Te-Te bonds and KS states in this region [see also Fig. 3(b)].

IV. CONCLUDING REMARKS

DF/MD simulations of the as-deposited phase of a-GST (AD, 648 atoms, >200 ps) have been compared with those for the melt-quenched structure (MQ, 460 atoms).[18]

Ge atoms have crucially different environments: predominantly tetrahedral in AD and (distorted) octahedral in MQ. The PBEsol functional gives improved results, and we can explain the apparent contradiction between the Ge-Te distances measured (EXAFS) and calculated. "Wrong bonds" in AD reduce the number of $ABAB$ squares, which nucleate during crystallization. Their absence in AD explains the much slower phase transition. Te-Te bonds are not favored in AD and MQ, and the latter is more stable by 11 meV/atom. The energetic ordering is consistent with the experimental fact that AD only exists up to the start of crystallization. The structure factor and electronic properties are very similar, and distinguishing between them using XRD is difficult: EXAFS and XANES are valuable alternatives.

ACKNOWLEDGMENTS

The calculations were performed on the Jugene (IBM Blue Gene/P) and Juropa (Intel Xeon 5570) computers in the FZ Jülich with grants from the FZJ and the John von Neumann Institute for Computing (NIC). We thank A. Filipponi for calculating EXAFS from our partial PDF, S. Kohara, T. Matsunaga, and N. Yamada for discussions and support, and the Academy of Finland for funding.

[1] K. J. Dawson, K. L. Kearns, L. Yu, W. Steffen, and M. D. Ediger, Proc. Nat. Acad. Sci. USA **106**, 15165 (2009).
[2] G. Dale, P. J. S. Ewen, and A. E. Owen, J. Non-Cryst. Solids, **256–257**, 348 (1999).
[3] S. Tsunashima, S. Mitsuya, and S. Uchiyama, Jpn. J. Appl. Phys. **20**, 727 (1981).
[4] M. Wuttig and N. Yamada, Nature Mater. **6**, 824 (2007), and references therein.
[5] J. H. Coombs, A. P. J. M. Jongenelis, W. van Es-Spiekman, and B. A. J. Jacobs, J. Appl. Phys. **78**, 4906 (1995).
[6] J. Park, M. R. Kim, W. S. Choi, H. Seo, and C. Yeon, Jpn. J. Appl. Phys. **38**, 4775 (1999).
[7] P. K. Khulbe, E. M. Wright, and M. Mansurpir, J. Appl. Phys. **88**, 3926 (2000).
[8] S. Raoux, H.-Y. Cheng, M. A. Caldwell, and H.-S. P. Wong, Appl. Phys. Lett. **95**, 071910 (2009).
[9] A. V. Kolobov, P. Fons, A. I. Frenkel, A. L. Ankudinov, J. Tominaga, and T. Uruga, Nature Mater. **3**, 703 (2004).
[10] D. A. Baker, M. A. Paesler, G. Lucovsky, S. C. Agarwal, and P. C. Taylor, Phys. Rev. Lett. **96**, 255501 (2006); M. A. Paesler, D. A. Baker, G. Lucovsky, A. E. Edwards, and P. C. Taylor, J. Phys. Chem. Solids **68**, 873 (2007).
[11] P. Jovari, I. Kaban, J. Steiner, B. Beuneu, A. Schöps, and A. Webb, J. Phys. Condens. Matter **19**, 335212 (2007).
[12] S. Kohara, K. Kato, S. Kimura, H. Tanaka, T. Usuki, K. Suzuya, H. Tanaka, Y. Moritomo, T. Matsunaga, N. Yamada, Y. Tanaka, H. Suematsu, and M. Takata, Appl. Phys. Lett. **89**, 201910 (2006).
[13] J.-J. Kim, K. Kobayashi, E. Ikenaga, M. Kobata, S. Ueda, T. Matsunaga, K. Kifune, R. Kojima, and N. Yamada, Phys. Rev. B **76**, 115124 (2007).
[14] J. Akola and R. O. Jones, Phys. Rev. B **76**, 235201 (2007); J. Phys. Condens. Matter **20**, 465103 (2008); Phys. Rev. Lett. **100**, 205502 (2008); Phys. Rev. B **79**, 134118 (2009).
[15] S. Caravati, M. Bernasconi, T. D. Kühne, M. Krack, and M. Parrinello, Appl. Phys. Lett. **91**, 171906 (2007).
[16] J. Hegedüs and S. R. Elliott, Nature Mater. **7**, 399 (2008).
[17] K. B. Borisenko, Y. Chen, S. A. Song, and D. J. H. Cockayne, Chem. Mater. **21**, 5244 (2009).
[18] J. Akola, R. O. Jones, S. Kohara, S. Kimura, K. Kobayashi, M. Takata, T. Matsunaga, R. Kojima, and N. Yamada, Phys. Rev. B **80**, 020201(R) (2009).
[19] M. Xu, Y. Q. Cheng, H. W. Sheng, and E. Ma, Phys. Rev. Lett. **103**, 195502 (2009).
[20] M. Naito, M. Ishimaru, Y. Hirotsu, R. Kojima, and N. Yamada, J. Appl. Phys. **107**, 103507 (2010).
[21] CPMD V3.13 Copyright IBM Corp. 1990–2009, Copyright MPI für Festkörperforschung Stuttgart 1997–2001 [http://www.cpmd.org].
[22] N. Troullier and J. L. Martins, Phys. Rev. B **43**, 1993 (1991).
[23] J. P. Perdew, A. Ruzsinszky, G. I. Csonka, O. A. Vydrov, G. E. Scuseria, L. A. Constantin, X. Zhou, and K. Burke, Phys. Rev. Lett. **100**, 136406 (2008).
[24] G. J. Martyna, M. L. Klein, and M. Tuckerman, J. Chem. Phys. **97**, 2635 (1992).
[25] J. Kolafa, J. Comput. Chem. **25**, 335 (2004).
[26] Fourfold coordinated Ge atoms are "tetrahedral" if the average deviation of *all* six bond angles (for bonds $\leqslant 3.0$ Å) from the octahedral values (90° and 180°) exceeds 10°.
[27] B. Huang and J. Robertson, Phys. Rev. B **81**, 081204(R) (2010).
[28] A. Filipponi, J. Phys. Condens. Matter **13**, R23 (2001).
[29] A. Filipponi, A. Di Cicco , and C. R. Natoli, Phys. Rev. B **52**, 15122 (1995).